

Proximity effects and a topological invariant in a Chern insulator connected to leads

Satyam Sinha,^{1,2} Rekha Kumari,¹ Junaid Majeed Bhat,³ Abhishek Dhar,¹ and R. Shankar⁴

¹*International Center for Theoretical Sciences (ICTS), Bengaluru, India*

²*Department of Physics, Indian Institute of Science Education and Research, Pune 411008, India*

³*University of Kashmir, Kupwara Campus, Wayen, Kupwara-193222, India*

⁴*The Institute of Mathematical Sciences, C I T Campus, Chennai 600 113, India*

The observed robustly quantized Hall conductance in quantum Hall systems and Chern insulators (CI) have so far been understood in terms of the topology of isolated systems, which are not coupled to leads. It is assumed that the leads act as inert reservoirs that simply supply/absorb electrons to/from the sample. Within a model of a CI coupled to leads with a cylindrical geometry, we show that this is not true. In the proximity of the CI, the edge current leaks into the leads, with the Hall conductance quantized only if this novel proximity effect is taken into account. For a special choice of leads, we identify the conductance with a topological invariant of the system, in terms of the winding number of the phase of the reflection coefficients of the scattering states.

Introduction: Insulators with non-trivial topology (INT) support chiral edge modes that carry dissipationless currents [1, 2]. This property makes them have potential applications in fields such as quantum computation and spintronics [3, 4]. Therefore, topological phases have naturally taken an important place in the field of condensed matter physics and are currently studied extensively [5, 6].

INTs owe their birth to the observation of the quantum Hall effect in the 1980's [7]. Quantum Hall phases are the first topological phases that were discovered experimentally. Later, many other models characterized by different topological invariants and with experimental realizations were developed in one, two, and three dimensions [8–16]. Broadly classified, we now have insulators that break time reversal symmetry (TRS), referred to as Chern Insulators (CIs), and insulators that possess time reversal symmetry, referred to as Z_2 topological insulators (TI) which have pairs of counter-propagating edge states. These states are symmetry-protected topological states, so the associated edge currents are robust against impurity scattering [17–19]. INTs are characterized by topological invariants that depend on the symmetries of the system [20–22].

The work of Laughlin [23] and Halperin [24] were the first to provide a theoretical understanding of QHE and point out the importance of edge states. The identification of the Hall conductance with a topological invariant, namely the Chern number, was obtained by TKNN [25], and this was later extended to interacting and disordered systems [26]. These results were obtained for the system in a torus geometry. For a cylindrical geometry, Hatsugai [27] showed that the Hall conductance is related to a topological invariant which is equal to the number of chiral edge channels intersecting the Fermi level at each edge.

All the above work concentrated on the topology of isolated systems. TKNN used the Green-Kubo formalism for isolated systems with periodic boundary conditions, while Hatsugai used the Laughlin-Halperin setup, which assumes reservoirs that are passive sources/sinks of electrons. It is not clear how these results are affected once

one considers the experimental setup of the INT connected to metallic leads. For instance, the TKNN result in Ref. [25] expresses the Hall conductivity in terms of the eigenstates of the isolated system; however, in the presence of leads, we expect that the scattering states dictate the transport, and their form depends on the details of the leads and their coupling to the system.

For TIs connected to leads, in two dimensions, a quantized transmission in two-terminal geometries has been proposed to be a signal for the non-trivial Z_2 invariant [28, 29]. The quantization of the two-terminal conductance has been demonstrated numerically in various studies [30, 31] and also in experiments [32, 33]. The quantization is justified using the Landauer-Buttiker formalism while assuming single-channel leads and perfect point contacts between the leads and the edge states of the TI [28, 34–36]. A recent study provides a microscopic justification for these assumptions using the non-equilibrium Green's function (NEGF) approach [37]. The striking form of current patterns (equivalently scattering states) inside the leads, was pointed out. A complete understanding is still lacking.

In this Letter, we consider the Hall conductance of a CI connected to leads. We consider the cylindrical geometry similar to that used in the Laughlin argument [23, 27] where a time-dependent unit flux threaded through the cylinder causes a quantized charge transfer across the edges of the cylinder. In contrast, here we consider a static setup where a voltage bias is applied to leads at the two ends of the CI and a Hall current is induced in the azimuthal direction at the edges.

We employ the microscopic formalisms of NEGF [35, 38–41] and scattering theory to compute the Hall conductance of a CI connected to metallic leads (see Fig. (1)). Here we summarize the most important results:

(i) Using the cylindrical symmetry of the problem and transfer matrix methods, we obtain a closed form expression, Eq. (5), for the Hall conductance in the thermodynamic limit.

(ii) For a particular choice of leads (disconnected 1D wires), we show that the Hall conductance can be expressed as a winding number and hence is quantized. It

is non-vanishing only in the phase with a non-vanishing Chern number. We interpret this winding number as the winding number of the phase of the reflection coefficients in the manifold of occupied scattering states.

(iii) For general leads, the scattering states for a single metal-CI junction are obtained analytically (Eq. (7)), and we find that, except for the special case of 1D leads, the Hall current leaks into the leads. This is surprising since the isolated lead has TRS. It is due to the coupling with the CI, which breaks TRS - we call this a proximity effect. Using the scattering states solution, we obtain the local Hall conductance, Eq. (9), in both lead and CI and show numerically that the total is still quantized. We also numerically demonstrate the equivalence of the results from scattering and NEGF formalisms, as expected [40].

We now present the crucial steps in the calculations. The complete details are provided in the Appendices.

The Model: We consider the two dimensional (2D) spinless Bernevig-Hughes-Zhang (SBHZ) model [6, 29] on a cylindrical lattice of size $N_x \times N_y$. Periodic boundary conditions are applied along the y -direction, and semi-infinite metallic leads are attached at the boundaries in the x direction, as shown in Fig. 1(a). Thus, the Hamiltonian of the full system is given by, $\mathcal{H}_{\text{total}} = \mathcal{H}^S + \mathcal{H}^L + \mathcal{H}^R + \mathcal{H}^{SL} + \mathcal{H}^{SR}$, where \mathcal{H}^S is the Hamiltonian of the SBHZ wire,

$$\begin{aligned} \mathcal{H}^S = & \sum_{x,y=1}^{N_x, N_y} \mu_w \mathbf{c}^\dagger(x, y) \sigma_x \mathbf{c}(x, y) \\ & + \eta \sum_{x=1}^{N_x} \sum_{y=1}^{N_y} \left[\mathbf{c}^\dagger(x, y) \frac{1}{2} (\sigma_x - i\sigma_z) \mathbf{c}(x, y+1) + h.c. \right] \\ & + \eta \sum_{x=1}^{N_x-1} \sum_{y=1}^{N_y} \left[\mathbf{c}^\dagger(x, y) \frac{1}{2} (\sigma_x - i\sigma_y) \mathbf{c}(x+1, y) + h.c. \right], \end{aligned} \quad (1)$$

where $\mathbf{c}(x, y) = (c_1(x, y), c_2(x, y))^T$, with $c_1(x, y)$ and $c_2(x, y)$ denoting the fermionic annihilation operators corresponding to the two orbital degrees of freedom at lattice site (x, y) . Henceforth we work in units with $\eta = 1$ and $e = \hbar = 1$. The matrices σ_x , σ_y , and σ_z are the usual Pauli matrices. For $0 < \mu_w < 2$ and $-2 < \mu_w < 0$, the isolated SBHZ model on a torus exhibits topologically nontrivial phases with Chern numbers $\mathcal{C} = +1$ and $\mathcal{C} = -1$, respectively. For isolated model on a cylinder, in these phases, the bulk band gap hosts edge states that are localized along the system boundaries and carry dissipationless chiral currents [1, 42]. The Hamiltonians of the left and right leads are denoted by \mathcal{H}^L and \mathcal{H}^R and modeled by nearest-neighbor tight-binding 2D lattices with hopping amplitudes, η_x and η_y , in the longitudinal and transverse directions, respectively. The leads are connected to the boundary sites of the SBHZ model, as shown in Fig. 1(a). The contacts are described by tight-binding Hamiltonians with hopping amplitude η_c .

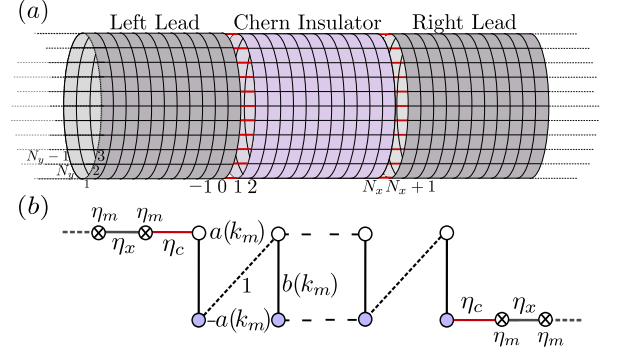


FIG. 1. (a) Schematic of a Chern insulator connected to metallic leads in the cylindrical geometry. (b) Equivalent Rice-Mele type one-dimensional setup obtained after Fourier transforming along the y -direction. The crossed sites indicate the sites belonging to the leads. The parameters a_m and η_m indicate onsite potentials in the CI and lead respectively, b_m and η_x are hopping terms in the CI and lead respectively, and η_c is the CI-lead coupling.

Details of the lead and coupling Hamiltonians are provided in the Appendix B.

The cylindrical geometry, and translational invariance in the y -direction, allows us to perform a Fourier transform, which reduces the problem to that of a set of decoupled one-dimensional chains (see Appendix B), each chain consisting of a 1D system coupled to 1D leads. We denote the single-particle system Hamiltonian of the m th chain as \tilde{H}_m^S ($m = 1, 2, \dots, N_y$) — we find that it has the form of the Rice-Mele model [43, 44], with a staggered onsite potential $a(k_m) = \sin k_m$ and alternating hopping amplitudes, $b(k_m) = \mu_w + \cos k_m$ and 1, with $k_m = 2\pi m/N_y$, as illustrated in Fig. 1(b). The effective 1D leads have an onsite potential $\eta_m = 2\eta_y \cos k_m$ and a nearest neighbor hopping η_x .

NEGF expression for the Hall Conductance: In the NEGF formalism, all currents and densities can be obtained from the steady-state two-point correlation matrix of the wire, $C_{x,y,s;x',y',s'} = \langle c_s^\dagger(x, y) c_{s'}(x', y') \rangle$. Here, $\langle \cdot \rangle$ denotes the expectation value in the steady state and s, s' label the orbital degrees of freedom of the CI. Thus the current along the bond connecting sites $\mathbf{x} = (x, y)$ and $\mathbf{x}' = (x', y')$ is given as $J_{\mathbf{x};\mathbf{x}'} = -2 \sum_{s,s'=1}^2 \text{Im} [H^S[\mathbf{x}, s; \mathbf{x}', s'] C_{\mathbf{x},s;\mathbf{x}',s'}]$. We are interested in the total current along the y direction, given by $J_y = \sum_{x=1}^{N_x} J_{x,y;x,y+1}$. Here we focus on the zero-temperature case ($T_L = T_R = 0$) and restrict ourselves to the linear-response regime with an infinitesimal bias in the chemical potential, μ , across the leads. The Hall conductance is given by $G_H(\mu) = \partial J_y / \partial \mu$. Using the decomposition of the system into a set of 1D chains, all steady state properties of the CI can be expressed in terms of the effective single-particle Green's function of the decoupled wires:

$$\tilde{\mathcal{G}}^m(\omega) = \frac{1}{\omega - \tilde{H}_m^S - \tilde{\Sigma}_m^L(\omega) - \tilde{\Sigma}_m^R(\omega)}, \quad (2)$$

where $\tilde{\Sigma}_m^L(\omega)$ and $\tilde{\Sigma}_m^R(\omega)$ are the self-energies due to the left and right leads, respectively. Note that the Green's function matrix $\tilde{\mathcal{G}}^m(\mu)$ is a $2N_x \times 2N_x$ matrix, whose elements are denoted by $[\tilde{\mathcal{G}}^m(\mu)]_{x,s;x',s'}$. Since the contacts between the Chern insulator and the leads involve only nearest-neighbor coupling, the only nonzero self-energy elements are $[\tilde{\Sigma}_m^R(\omega)]_{1,1}$ and $[\tilde{\Sigma}_m^L(\omega)]_{2N_x,2N_x}$, and we denote these by $\Sigma_m(\omega) = \Lambda_m(\omega) + i\gamma_m(\omega)$. Using the procedure detailed in Appendix C, we obtain:

$$G_H = \frac{2}{N_y} \sum_{x=1}^{N_x} \sum_{m=1}^{N_y} \gamma_m(\mu) \mathbf{g}_{x1}(k_m) R(k_m) \mathbf{g}_{x1}(k_m), \quad (3)$$

where $\mathbf{g}_{x1}(k_m) = ([\tilde{\mathcal{G}}^m(\mu)]_{x,1;1,1} [\tilde{\mathcal{G}}^m(\mu)]_{x,2;1,1})^T$ and $R(k_m) = \sigma_z \cos k_m - \sigma_x \sin k_m$. We now use the transfer matrix approach to obtain the matrix elements of the Green's function, $\mathbf{g}_{x1}(k_m)$, that appear in Eq. (3). This approach provides an iterative scheme to analytically obtain the matrix elements of the Green's function [38, 41] and also has been previously used to study topological systems [27, 45–47]. Using this approach, we express \mathbf{g}_{x1} in terms of \mathbf{g}_{N_x1} as $\mathbf{g}_{x1} = [\Omega(\mu, k_m)]^{N_x-x} \mathbf{g}_{N_x1}$. The matrix $\Omega(\mu, k_m)$ is a 2×2 matrix with unit determinant that represents the bulk transfer matrix of the Chern insulator [48]. Its eigenvalues determine the nature of the eigenstates of the system. Complex eigenvalues of unit modulus correspond to extended states, whereas real eigenvalues correspond to states localized at the edges. The transfer-matrix approach also yields $\mathbf{g}_{N_x1} = g_{N_x1}^{(2)} \boldsymbol{\xi}_m$, where $\boldsymbol{\xi}_m = ((\mu + a(k_m) - \Sigma_m(\mu))/b(k_m) \ 1)^T$ and $g_{N_x1}^{(2)} = [(\Omega_L \Omega^{N_x-1} \Omega_R)^{-1}]_{11}$. Here, Ω_L and Ω_R are boundary transfer matrices that contain the details of the lead Hamiltonians and their coupling to the Chern insulator (the derivation is presented in Appendix D). Using the results for \mathbf{g}_{x1} in Eq. (3), we obtain

$$G_H(\mu) = \frac{2}{N_y} \sum_{m=1}^{N_y} \gamma_m \boldsymbol{\xi}_m^\dagger M(\mu, k_m) \boldsymbol{\xi}_m, \quad (4)$$

where $M(\mu, k_m) = |g_{N_x1}^{(2)}|^2 \sum_{x=1}^{N_x} (\Omega^T)^{N_x-x} R(k_m) \Omega^{N_x-x}$. For μ in the band gap, the sum in Eq. (4) converges in the limit $N_x, N_y \rightarrow \infty$ to the following simplified expression:

$$G_H(\mu) = \frac{1}{\pi} \int_0^{2\pi} \frac{\gamma(\mu, k)}{\gamma^2(\mu, k) + g^2(\mu, k)} h(\mu, k) dk, \quad (5)$$

where $\gamma_m(\mu) \rightarrow \gamma(\mu, k)$, $\Lambda_m(\mu) \rightarrow \Lambda(\mu, k)$, $g(\mu, k) = (a - \mu) + \Lambda + bf$ and $h(\mu, k) = [(b - \mu_w)(1 - f^2 - 2af)/(1 - \lambda_1^2)]$, with $f(\mu, k) = (\mu - a)/(\lambda_2 + b)$, and $|\lambda_1| < |\lambda_2|$ are the two eigenvalues of $\Omega(\mu, k)$ (See Appendix D for details).

Special choice of leads: We now consider the case of the lead consisting of uncoupled 1D wires, which corresponds to the choice $\eta_y = 0$. For this choice one easily sees that γ and Λ have no k dependence and a direct computation shows that $dg(\mu, k)/dk = h(\mu, k)$. This allows us to express Eq. (5) as,

$$G_H(\mu) = \frac{1}{2\pi} \int_0^{2\pi} \frac{d\phi(\mu, k)}{dk} dk, \quad (6)$$

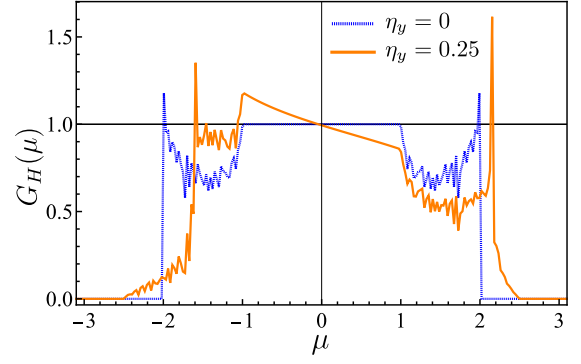


FIG. 2. Variation of the Hall conductance $G_H(\mu)$ with chemical potential μ for two different models of leads: (i) 1D case with $\eta_x = 1, \eta_y = 0$ and (ii) case with $\eta_x = 1, \eta_y = 0.25$. For (i), we see a quantized plateau of unit value in the bulk gap of the Chern insulator, while for (ii), we do not see quantization. Other parameters: $\mu_w = 1, \eta_c = 1$.

where $\phi(\mu, k) = 2 \tan^{-1} \left[\frac{(a-\mu)+\Lambda+bf}{\gamma} \right]$. This implies that $\phi(\mu, k + 2\pi) = \phi(\mu, k) + 2\pi n$, where n is an integer. Consequently, it implies that the RHS of Eq. (6) is an integer (see Appendix E for details). We find that it is equal to ± 1 in the topological regime ($|\mu_w| < 2$) and zero otherwise. It is important to note that $\phi(\mu, k)$ depends on both system and reservoir properties. Below, we relate it to the phase of the reflection coefficients of the scattering states.

In Fig. 2, we plot $G_H(\mu)$ obtained numerically from Eq. (3) (with parameters in the topological regime) as a function of the Fermi level μ . For the case of 1D leads ($\eta_y = 0$), we observe a quantized plateau of unit conductance when the Fermi level is in the band gap of the CI. We also show the results for the case $\eta_y \neq 0$ — surprisingly, we find that G_H , as given by Eqs. (3) or Eq. (5), is no longer quantized.

We now provide an understanding of the non-quantization of the Hall conductance by showing that, for general leads, a part of the Hall current in fact leaks into the metal. This is not included in the NEGF formula in Eq. (6). We will find that including this contribution restores quantization. While it is straightforward to compute currents in the leads using NEGF, we here use the equivalent approach of computing currents using scattering states. In the $N_x \rightarrow \infty$ limit being considered here, the mid-gap states incident from the left and right form localized edge states that are independent of each other — hence for the corresponding scattering states, it is sufficient to consider the lead-CI junction.

Scattering states for the single lead-CI junction: We focus on the scattering eigenstates with energies in the band gap of the CI. These arise from the hybridization of the edge modes of the Chern insulator with the eigenstates of the lead. For the cylindrical geometry, the scattering states can be labeled by x -momentum $q \in (0, \pi)$ and y -momentum $k \in (0, 2\pi)$ of the incoming electrons with energy $\epsilon_{q,k} = 2\eta_x \cos q + 2\eta_y \cos k$. As

detailed in Appendix F 1, this parameter space is geometrically a cylinder, periodic in the k direction and open in the q direction. The scattering states are of the form $\zeta_{q,k}(x, y) = \Psi_{q,k}(x)e^{iky}$, where

$$\Psi_{q,k}(x) = \begin{cases} e^{iqx} + r e^{-iqx}, & x \leq 0, \\ \begin{pmatrix} u \\ v \end{pmatrix} \lambda^{x-1}, & x > 0, \end{cases} \quad (7)$$

where the unknown amplitudes u , v , λ and r can be determined by solving the eigenvalue equation $H_k \Psi_{q,k} = \epsilon \Psi_{q,k}$, where H_k is the single-particle Hamiltonian of the effective one-dimensional lead-CI system.

We get explicit expressions for all parameters in the scattering state in terms of (q, k) . In particular, we find that $r(q, k) = e^{i\chi(q, k)}$, namely no transmission. Also, $u(q, k) = |u(q, k)|e^{\frac{i}{2}\chi(q, k)}$, $v(q, k) = |v(q, k)|e^{\frac{i}{2}\chi(q, k)}$. Further, we find that $\phi(\epsilon, k) = \chi(q, k) + 2q$, implying that $\partial_k \phi(\epsilon, k) = \partial_k \chi(q, k)$ (See Eq. (F17)).

For a given scattering state, the local Hall current at fixed x can be obtained from the following current operator for the 1D chains:

$$\hat{J}_y = \begin{cases} \sigma_z \cos k - \sigma_x \sin k, & \text{for } x > 0 \\ -2\eta_y \sin k, & \text{for } x \leq 0 \end{cases} \quad (8)$$

Summing over scattering states chosen from a filled Fermi sea, up to the energy level μ , gives us the local Hall conductance as:

$$\begin{aligned} \tilde{G}_H(\mu, x) &= \int_0^{q_F} \frac{dk}{2\pi} \int_0^{2\pi} dq \Psi_{q,k}^\dagger(x) \hat{J}_y \Psi_{q,k}(x) \delta(\mu - \epsilon_{q,k}) \\ &= \begin{cases} \frac{1}{\pi} \int_0^{2\pi} dk \frac{\gamma(\mu, k) \lambda_1^{2(x-1)} [(1-f^2) \cos k - 2af]}{\gamma^2(\mu, k) + g^2(\mu, k)}, & \text{for } x > 0 \\ \frac{-2\eta_y}{\pi} \int_0^{2\pi} dk \frac{\sin k \cos(2qx - \chi(q, k))}{\sqrt{4\eta_x^2 - (\mu - 2\eta_y \cos k)^2}}, & \text{for } x \leq 0. \end{cases} \end{aligned} \quad (9)$$

From this one can find the Hall conductance in the lead, $G_H^{\text{lead}}(\mu) = \sum_{x=-\infty}^0 \tilde{G}_H(\mu, x)$, and in the CI, $G_H^{\text{CI}}(\mu) = \sum_{x=1}^{\infty} \tilde{G}_H(\mu, x)$ (See Appendix F 2 for details). We now present numerical results for the case of general leads with $\eta_y \neq 0$. The main plot in Fig. (3) shows the contributions of the lead and CI parts to Hall conductance at different chemical potentials. Remarkably we see that the sum of their contributions again shows quantization. In the inset of Fig. (3) we plot $\tilde{G}_H(\mu, x)$ as a function of x and see that it is non-vanishing in the leads — we refer to this induced Hall conductance in the lead as a proximity effect. We also find that results obtained from the scattering formula show perfect agreement with NEGF results (obtained numerically for large N_y), as expected from the equivalence between the two formalisms [38, 40, 41].

For 1D leads ($\eta_y = 0$) we see that $G_H^{\text{lead}}(\mu)$ vanishes while $G_H^{\text{CI}}(\mu)$ is identical to the NEGF expression Eq. (5) and so is quantized (see Appendix E). The phase $\phi(\mu, k)$ defined in Eq. (6) is related to the phase of the phase

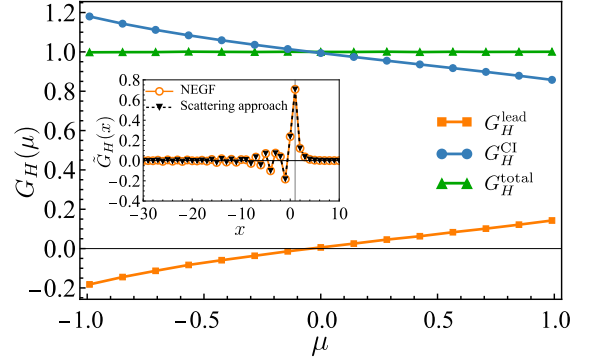


FIG. 3. Contributions to the Hall conductance from the CI and metallic leads are plotted as a function of the chemical potential for 2D leads. The inset shows the equivalence of local Hall conductance computed using the NEGF formalism and scattering approach for the 2D leads case. For both plots, $\mu_w = 1$, $\eta_x = 1$, $\eta_y = 0.25$, $\eta_c = 1$. For the inset $\mu = 0.8$.

reflection coefficient as, $\partial_k \phi(\epsilon, k) = \partial_k \chi(q, k)$. Hence, the topological invariant, for the 1D leads case, is the winding number of the phase of the reflection coefficients, as it winds around in the parameter space of the occupied scattering states. It is therefore a topological invariant of the S-matrix of the system.

The TKNN result relates the Hall conductance to the Berry phase of the Bloch wave functions of an isolated, periodic Chern insulator. In contrast, in our formulation, the winding number in Eq. (6) explicitly depends on the lead self-energy parameters Λ and γ and is directly related to the phase of the reflection coefficient of the scattering states. This reflects the influence of the leads on the transport and suggests that the winding number here should be interpreted as a topological invariant constructed from the scattering states of the open system, rather than from the eigenstates of the isolated CI. Namely, as a property of the S-Matrix of the system.

Conclusion and Outlook: We have addressed the quantization of Hall conductance in a 2D Chern insulator model in contact with metallic leads. Using the microscopic NEGF approach for a two-terminal setup and the equivalent scattering theory approach, we show that the Hall conductance is quantized, provided one includes contributions to the Hall current in the leads. Our exact solution of scattering states for a single lead-CI junction allows us to write a closed-form expression for the local Hall conductance. For the special case of 1D leads, we explicitly show that this is equal to the winding number of the phase of the reflection coefficient as it winds around the manifold of the occupied scattering states. Thus, our result extends the TKNN result to Lead-CI-Lead systems and suggests that the topological invariant identified with the observed quantized Hall conductance may be best expressed in terms of the S-Matrix for open systems.

Our findings are based on computations for a specific

model; generalizing this result to other models of system and leads, and exploring connections of the open system Hall-conductance with the Ishikawa-Matsuyama topological invariant [49–52] is an interesting open question. Also, experimental modeling of topological insulators in the cylindrical geometry is now possible by using the idea of synthetic dimensions in ultra-cold atoms [53–57]. It would be interesting to test our results in such experimental setups.

ACKNOWLEDGEMENTS

We thank Bijay Kumar Agarwalla, Ankush Chaubey, Abhinav Dhawan, Ashoke Sen, Joel Moore and Dipti-

man Sen for very helpful discussions. SS acknowledges the Long Term Visiting Students Program for supporting the visit to ICTS. AD acknowledges the J.C. Bose Fellowship (JCB/2022/000014) of the Science and Engineering Research Board of the Department of Science and Technology, Government of India. SS, RK and AD acknowledge the support of the DAE, Government of India, under projects nos. 12-R&D-TFR-5.10-1100 and RTI4001.

-
- [1] B. A. Bernevig and T. L. Hughes, Topological insulators and topological superconductors, in *Topological Insulators and Topological Superconductors* (Princeton University Press, 2013).
 - [2] Y. Tokura, M. Kawasaki, and N. Nagaosa, Emergent functions of quantum materials, *Nature Phys.* **13**, 1056 (2017).
 - [3] J. E. Moore, The birth of topological insulators, *Nature* **464**, 194 (2010).
 - [4] M. König, H. Buhmann, L. W. Molenkamp, T. L. Hughes, C.-X. Liu, X.-L. Qi, and S.-C. Zhang, The quantum spin hall effect: Theory and experiment, *J. Phys. Soc. Jpn.* **77**, 031007 (2008).
 - [5] M. Z. Hasan and C. L. Kane, Colloquium: Topological insulators, *Rev. Mod. Phys.* **82**, 3045 (2010).
 - [6] X.-L. Qi and S.-C. Zhang, Topological insulators and superconductors, *Rev. Mod. Phys.* **83**, 1057 (2011).
 - [7] K. von Klitzing, G. Dorda, and M. Pepper, New method for high-accuracy determination of the fine-structure constant based on quantized hall resistance, *Phys. Rev. Lett.* **45**, 494 (1980).
 - [8] F. D. M. Haldane, Model for a quantum hall effect without landau levels: Condensed-matter realization of the “parity anomaly”, *Phys. Rev. Lett.* **61**, 2015 (1988).
 - [9] C. L. Kane and E. J. Mele, Quantum spin hall effect in graphene, *Phys. Rev. Lett.* **95**, 226801 (2005).
 - [10] C. L. Kane and E. J. Mele, Z₂ topological order and the quantum spin hall effect, *Phys. Rev. Lett.* **95**, 146802 (2005).
 - [11] L. Fu, C. L. Kane, and E. J. Mele, Topological insulators in three dimensions, *Phys. Rev. Lett.* **98**, 106803 (2007).
 - [12] M. König, S. Wiedmann, C. Brüne, A. Roth, H. Buhmann, L. W. Molenkamp, X. Qi, and S. Zhang, Quantum spin hall insulator state in hgte quantum wells, *Science* **318**, 766 (2007).
 - [13] H. Zhang, C.-X. Liu, X.-L. Qi, X. Dai, Z. Fang, and S.-C. Zhang, Topological insulators in bi₂se₃, bi₂te₃ and sb₂te₃ with a single dirac cone on the surface, *Nature Phys.* **5**, 438 (2009).
 - [14] D. Hsieh, Y. Xia, D. Qian, L. A. Wray, J. H. Dil, F. Meier, J. Osterwalder, L. Patthey, J. G. Checkelsky, N. P. Ong, A. V. Fedorov, H. Lin, A. Bansil, D. C. Grauer, Y. S. Hor, R. J. Cava, and M. Z. Hasan, A tunable topological insulator in the spin helical dirac transport regime, *Nature* **460**, 1101 (2009).
 - [15] R. Roy, Topological phases and the quantum spin hall effect in three dimensions, *Phys. Rev. B* **79**, 195322 (2009).
 - [16] J. E. Moore and L. Balents, Topological invariants of time-reversal-invariant band structures, *Phys. Rev. B* **75**, 121306(R) (2007).
 - [17] G. Schubert, H. Fehske, L. Fritz, and M. Vojta, The fate of topological-insulator surface states under strong disorder, *Phys. Rev. B* **85**, 201105(R) (2012).
 - [18] H. Jiang, L. Wang, Q.-F. Sun, and X. C. Xie, Numerical study of the topological anderson insulator in hgte/cdte quantum wells, *Phys. Rev. B* **80**, 165316 (2009).
 - [19] C. Xu and J. E. Moore, Stability of the quantum spin hall effect: Effects of interactions, disorder, and Z₂ topology, *Phys. Rev. B* **73**, 045322 (2006).
 - [20] A. Kitaev, Periodic table for topological insulators and superconductors, *AIP Conf. Proc.* **1134**, 22 (2009).
 - [21] S. Ryu, A. P. Schnyder, A. Furusaki, and A. W. W. Ludwig, Topological insulators and superconductors: Tenfold way and dimensional hierarchy, *New J. Phys.* **12**, 065010 (2010).
 - [22] A. Agarwala, A. Haldar, and V. B. Shenoy, The tenfold way redux: Fermionic systems with n -body interactions, *Ann. Phys.* **385**, 469 (2017).
 - [23] R. B. Laughlin, Quantized hall conductivity in two dimensions, *Phys. Rev. B* **23**, 5632(R) (1981).
 - [24] B. I. Halperin, Quantized hall conductance, current-carrying edge states, and the existence of extended states in a two-dimensional disordered potential, *Phys. Rev. B* **25**, 2185 (1982).
 - [25] D. J. Thouless, M. Kohmoto, M. P. Nightingale, and M. den Nijs, Quantized hall conductance in a two-dimensional periodic potential, *Phys. Rev. Lett.* **49**, 405 (1982).
 - [26] Q. Niu, D. J. Thouless, and Y.-S. Wu, Quantized hall conductance as a topological invariant, *Phys. Rev. B* **31**, 3372 (1985).
 - [27] Y. Hatsugai, Edge states in the integer quantum hall effect and the riemann surface of the bloch function, *Phys. Rev. B* **48**, 11851 (1993).
 - [28] G. M. Gusev, Z. D. Kvon, E. B. Olshanetsky, and N. N. Mikhailov, Mesoscopic transport in two-dimensional

- topological insulators, *Solid State Commun.* **302**, 113701 (2019).
- [29] B. A. Bernevig, T. L. Hughes, and S.-C. Zhang, Quantum spin hall effect and topological phase transition in hgte quantum wells, *Science* **314**, 1757 (2006).
- [30] H. Huang and F. Liu, Quantum spin hall effect and spin bott index in a quasicrystal lattice, *Phys. Rev. Lett.* **121**, 126401 (2018).
- [31] A. Agarwala and V. B. Shenoy, Topological insulators in amorphous systems, *Phys. Rev. Lett.* **118**, 236402 (2017).
- [32] A. Roth, C. Brüne, H. Buhmann, L. W. Molenkamp, J. Maciejko, X.-L. Qi, and S.-C. Zhang, Nonlocal transport in the quantum spin hall state, *Science* **325**, 294 (2009).
- [33] C. Fuchs, S. Shamim, P. Shekhar, L. Fürst, J. Kleinlein, J. I. Väyrynen, H. Buhmann, and L. W. Molenkamp, Kondo interaction of quantum spin hall edge channels with charge puddles, *Phys. Rev. B* **108**, 205302 (2023).
- [34] J. K. Jain, *Composite Fermions* (Cambridge University Press, Cambridge; New York, 2007).
- [35] S. Datta, *Electronic Transport in Mesoscopic Systems* (Cambridge University Press, 1997).
- [36] G. Dolcetto, M. Sasseti, and T. L. Schmidt, Edge physics in two-dimensional topological insulators, *Rivista del Nuovo Cimento* **39**, 113 (2016).
- [37] J. M. Bhat, R. Shankar, and A. Dhar, Quantized two terminal conductance, edge states and current patterns in an open geometry 2-dimensional chern insulator, *J. Phys.: Condens. Matter* **37**, 275601 (2025).
- [38] D. Ryndyk, *Theory of Quantum Transport at Nanoscale: An Introduction*, Springer Series in Solid-State Sciences, Vol. 184 (Springer, 2016).
- [39] A. Dhar and D. Sen, Nonequilibrium green's function formalism and the problem of bound states, *Phys. Rev. B* **73**, 085119 (2006).
- [40] X. Waintal, M. Wimmer, A. R. Akhmerov, C. Groth, B. K. Nikolić, M. Istaş, T. Örn Rosdahl, and D. Varjas, Computational quantum transport, *arXiv:2407.16257* (2024).
- [41] J. M. Bhat and A. Dhar, Equivalence of NEGF and scattering approaches to electron transport in the kitaev chain, *arXiv: 2101.06376* (2021).
- [42] R. Shankar, Topological insulators — a review, *arXiv preprint* [10.48550/arXiv.1804.06471](https://arxiv.org/abs/10.48550/arXiv.1804.06471) (2018), [arXiv:1804.06471 \[cond-mat.str-el\]](https://arxiv.org/abs/1804.06471).
- [43] M. J. Rice and E. J. Mele, Elementary excitations of a linearly conjugated diatomic polymer, *Phys. Rev. Lett.* **49**, 1455 (1982).
- [44] J. K. Asbóth, L. Oroszlány, and A. Pályi, *A Short Course on Topological Insulators: Band Structure and Edge States in One and Two Dimensions*, Lecture Notes in Physics, Vol. 919 (Springer, 2016).
- [45] R. Wielan, I. Toftul, and Y. Kivshar, Transfer matrix approach for topological edge states, *Phys. Rev. B* **111**, 035151 (2025).
- [46] F. K. Kunst and V. Dwivedi, Non-hermitian systems and topology: A transfer-matrix perspective, *Phys. Rev. B* **99**, 245116 (2019).
- [47] J. Arkinstall, M. H. Teimourpour, L. Feng, R. El-Ganainy, and H. Schomerus, Topological tight-binding models from nontrivial square roots, *Phys. Rev. B* **95**, 165109 (2017).
- [48] V. Dwivedi and V. Chua, Of bulk and boundaries: Generalized transfer matrices for tight-binding models, *Phys. Rev. B* **93**, 134304 (2016).
- [49] K. Ishikawa and T. Matsuyama, A microscopic theory of the quantum hall effect, *Nucl. Phys. B* **280**, 523 (1987).
- [50] J.-H. Zheng and W. Hofstetter, Topological invariant for two-dimensional open systems, *Phys. Rev. B* **97**, 195434 (2018).
- [51] G. E. Volovik, *The universe in a helium droplet*, Vol. 117 (OUP Oxford, 2003).
- [52] V. Gurarie, Single-particle green's functions and interacting topological insulators, *Phys. Rev. B* **83**, 085426 (2011).
- [53] A. Celi, P. Massignan, J. Ruseckas, N. Goldman, I. B. Spielman, G. Juzeliūnas, and M. Lewenstein, Synthetic gauge fields in synthetic dimensions, *Phys. Rev. Lett.* **112**, 043001 (2014).
- [54] O. Boada, A. Celi, J. I. Latorre, and M. Lewenstein, Quantum simulation of an extra dimension, *Phys. Rev. Lett.* **108**, 133001 (2012).
- [55] J. H. Han, J. H. Kang, and Y. Shin, Band gap closing in a synthetic hall tube of neutral fermions, *Phys. Rev. Lett.* **122**, 065303 (2019).
- [56] C.-H. Li, Y. Yan, S.-W. Feng, S. Choudhury, D. B. Blas-ing, Q. Zhou, and Y. P. Chen, Bose-einstein condensate on a synthetic topological hall cylinder, *PRX Quantum* **3**, 010316 (2022).
- [57] A. Fabre, J.-B. Bouhiron, T. Satoor, R. Lopes, and S. Nascimbene, Laughlin's Topological Charge Pump in an Atomic Hall Cylinder, *Phys. Rev. Lett.* **128**, 173202 (2022).

Appendix A: Glossary of symbols

Symbol	Definition
μ_w	CI parameter
η_x	x -direction hopping strength in the leads
η_y	y -direction hopping strength in the leads
η_c	Coupling of leads to CI
$\epsilon(q, k)$	$2(\eta_x \cos q + \eta_y \cos k)$
$\Lambda(\omega, k)$	$\frac{\eta_c^2}{2\eta_x^2}(\omega - 2\eta_y \cos k)$
$\gamma(\omega, k)$	$-\frac{\eta_c^2}{2\eta_x^2}[4\eta_x^2 - (\omega - 2\eta_y \cos k)^2]^{1/2}$
$a(k)$	$\sin k$
$b(k)$	$\mu_w + \cos k$
$\Delta(q, k)$	$\frac{1}{b}(\epsilon^2 - a^2 - b^2 - 1)$
$\lambda(q, k)$	$\frac{1}{2}(\Delta \pm \sqrt{\Delta^2 - 4})$
$\lambda_1(q, k)$	λ if $ \lambda < 1$
$\lambda_2(q, k)$	λ if $ \lambda > 1$
$f(\mu, k)$	$(\epsilon - a)/(1/\lambda_1 + b)$
$g(\mu, k)$	$(a - \epsilon) + \Lambda + bf$
$c(q, k)$	$g - \Lambda$
$\phi(\mu, k)$	$2 \tan^{-1} \frac{g}{\gamma}$
$\chi(q, k)$	$-2 \arctan \left(\frac{c\Lambda + \eta_c^4 \eta_x^{-2}}{c\gamma} \right)$

Appendix B: Setup details and transformation to 1D chains

As mentioned in the main text, the Hamiltonian for the full system is given by :

$$\mathcal{H}_{\text{total}} = \mathcal{H}^S + \mathcal{H}^L + \mathcal{H}^R + \mathcal{H}^{SL} + \mathcal{H}^{SR}. \quad (\text{B1})$$

We recall that \mathcal{H}^S represents the Hamiltonian considered for the Chern insulator (CI) which is defined in the main text as follows,

$$\begin{aligned} \mathcal{H}^S = & \sum_{x,y=1}^{N_x, N_y} \mu_w \mathbf{c}^\dagger(x, y) \sigma_x \mathbf{c}(x, y) \\ & + \sum_{x=1}^{N_x} \sum_{y=1}^{N_y} \left[\mathbf{c}^\dagger(x, y) \frac{1}{2} (\sigma_x - i\sigma_z) \mathbf{c}(x, y+1) + h.c. \right] \\ & + \sum_{x=1}^{N_x-1} \sum_{y=1}^{N_y} \left[\mathbf{c}^\dagger(x, y) \frac{1}{2} (\sigma_x - i\sigma_y) \mathbf{c}(x+1, y) + h.c. \right], \end{aligned} \quad (\text{B2})$$

where $\mathbf{c}(x, y) = \begin{pmatrix} c_1(x, y) & c_2(x, y) \end{pmatrix}^T$. We recall from the main text that $c_1(x, y)$ and $c_2(x, y)$ are the fermionic annihilation operators corresponding to the two orbital degrees of freedom at lattice site (x, y) of the CI.

\mathcal{H}^L and \mathcal{H}^R represent the Hamiltonian of the left and right leads, respectively. \mathcal{H}^{SL} (\mathcal{H}^{SR}) represent the contacts between CI and the left (right) lead. The leads are modeled by the nearest-neighbor tight-binding Hamiltonians as follows,

nians as follows,

$$\begin{aligned} \mathcal{H}^L = & \sum_{x=-\infty}^{-1} \sum_{y=1}^{N_y} \eta_x [c_L^\dagger(x, y) c_L(x+1, y) + h.c.] \\ & + \sum_{x=-\infty}^0 \sum_{y=1}^{N_y} \eta_y [c_L^\dagger(x, y) c_L(x, y+1) + h.c.], \end{aligned} \quad (\text{B3})$$

$$\begin{aligned} \mathcal{H}^R = & \sum_{x=N_x+1}^{\infty} \sum_{y=1}^{N_y} \eta_x [c_R^\dagger(x, y) c_R(x+1, y) + h.c.] \\ & + \sum_{x=N_x+1}^{\infty} \sum_{y=1}^{N_y} \eta_y [c_L^\dagger(x, y) c_L(x, y+1) + h.c.], \end{aligned} \quad (\text{B4})$$

Here, $c_L(x, y)$ and $c_R(x, y)$ are fermionic annihilation operators in the left and right leads, respectively. η_x and η_y are the hopping amplitudes along the x and y direction, respectively. We have imposed periodic boundary conditions along the y -direction, therefore $c_{L/R}(x, N_y + 1) = c_{L/R}(x, 1)$. The contacts between CI and the leads are modelled by the following Hamiltonians,

$$\mathcal{H}^{SL} = \sum_{y=1}^{N_y} \eta_c [c_L^\dagger(0, y) c_1(1, y) + h.c.], \quad (\text{B5})$$

$$\mathcal{H}^{SR} = \sum_{y=1}^{N_y} \eta_c [c_2^\dagger(N_x, y) c_R(N_x + 1, y) + h.c.]. \quad (\text{B6})$$

Here, η_c is the coupling between the CI and the leads. Due to the translational symmetry along y -direction, $\mathcal{H}_{\text{total}}$ is block diagonal in the Fourier basis,

$$\tilde{\mathbf{c}}_m(x) = \frac{1}{\sqrt{N_y}} \sum_{y=1}^{N_y} e^{ik_m y} \mathbf{c}(x, y), \quad (\text{B7})$$

$$\tilde{c}_{L,m}(x) = \frac{1}{\sqrt{N_y}} \sum_{y=1}^{N_y} e^{ik_m y} c_L(x, y), \quad (\text{B8})$$

$$\tilde{c}_{R,m}(x) = \frac{1}{\sqrt{N_y}} \sum_{y=1}^{N_y} e^{ik_m y} c_R(x, y), \quad (\text{B9})$$

where $k_m = 2\pi m/N_y$ with $m = 1, 2, 3, \dots, N_y$. Using these operators we rewrite $\mathcal{H}_{\text{total}}$ as follows,

$$\tilde{\mathcal{H}}_{\text{total}} = \sum_{m=1}^{N_y} \tilde{\mathcal{H}}_m^S + \tilde{\mathcal{H}}_m^L + \tilde{\mathcal{H}}_m^R + \tilde{\mathcal{H}}_m^{SL} + \tilde{\mathcal{H}}_m^{SR}, \quad (\text{B10})$$

where,

$$\tilde{\mathcal{H}}_m^S = \sum_{x', x=1}^{N_x} \tilde{\mathbf{c}}_m^\dagger(x) \tilde{H}_m^S[x, x'] \tilde{\mathbf{c}}_m(x'). \quad (\text{B11})$$

Here, $\tilde{H}_m^S[x, x']$ is a 2×2 block of the $2N_x \times 2N_x$ matrix \tilde{H}_m^S which has the following matrix elements,

$$\tilde{H}_m^S = \begin{pmatrix} a(k_m) & b(k_m) & 0 & 0 & \cdots & 0 & 0 \\ b(k_m) & -a(k_m) & 1 & 0 & \cdots & 0 & 0 \\ 0 & 1 & a(k_m) & b(k_m) & \cdots & 0 & 0 \\ \vdots & \vdots & b(k_m) & -a(k_m) & \ddots & \vdots & \vdots \\ \vdots & \vdots & \vdots & \ddots & \ddots & 1 & 0 \\ \vdots & \vdots & \vdots & \cdots & 1 & a(k_m) & b(k_m) \\ 0 & 0 & 0 & \cdots & 0 & b(k_m) & -a(k_m) \end{pmatrix} \quad (\text{B12})$$

$$\begin{aligned} \tilde{H}_m^L &= 2\eta_y \cos k_m \sum_{x=-\infty}^0 \tilde{c}_{L,m}^\dagger(x) \tilde{c}_{L,m}(x), \\ &+ \sum_{x=-\infty}^{-1} \eta_x [\tilde{c}_{L,m}^\dagger(x) \tilde{c}_{L,m}(x+1) + \text{h.c.}] \end{aligned} \quad (\text{B13})$$

$$\begin{aligned} \tilde{H}_m^R &= 2\eta_y \cos k_m \sum_{x=N_x+1}^{\infty} \tilde{c}_{R,m}^\dagger(x) \tilde{c}_{R,m}(x) \\ &+ \sum_{x=N_x+1}^{\infty} \eta_x [\tilde{c}_{R,m}^\dagger(x) \tilde{c}_{R,m}(x+1) + \text{h.c.}], \end{aligned} \quad (\text{B14})$$

$$\tilde{H}_m^{SL} = \eta_c [\tilde{c}_{L,m}^\dagger(0) \tilde{c}_{1,m}(1) + \text{h.c.}], \quad (\text{B15})$$

$$\tilde{H}_m^{SR} = \eta_c [\tilde{c}_{2,m}^\dagger(N_x) \tilde{c}_{R,m}(N_x+1) + \text{h.c.}]. \quad (\text{B16})$$

where $a(k_m) = \sin k_m$ and $b(k_m) = \mu_w + \cos k_m$. Taking the partial Fourier transform of \mathcal{H}_S along the y -direction yields N_y decoupled 1D chains, with Hamiltonians \tilde{H}_m^S resembling the Rice–Mele model [43, 44, 48].

Appendix C: NEGF formalism in cylindrical geometry

The non-equilibrium steady state (NESS) properties of the system can be expressed in terms of the effective single particle Green's function of the system [39],

$$\mathcal{G}(\omega) = \frac{1}{\omega - H^S - \Sigma^L(\omega) - \Sigma^R(\omega)}, \quad (\text{C1})$$

where H^S is the single particle Hamiltonian of the isolated system, and $\Sigma^{L(R)}(\omega)$ represents the self-energy due to the left (right) lead. The Green's function is block diagonal in the basis given in Eq. (B7) and therefore its elements can be written as,

$$\mathcal{G}_{x,a,m;x',b,m'}(\omega) = \tilde{\mathcal{G}}_{x,a;x',b}^m(\omega) \delta_{m,m'}, \quad (\text{C2})$$

where,

$$\tilde{\mathcal{G}}^m = \frac{1}{\omega - \tilde{H}_m^S - \tilde{\Sigma}_m^L(\omega) - \tilde{\Sigma}_m^R(\omega)}, \quad (\text{C3})$$

and $\tilde{\Sigma}_m^L(\omega)$, $\tilde{\Sigma}_m^R(\omega)$ are the self energies of the decoupled chains:

$$[\tilde{\Sigma}_m^L]_{x,s;x',s'} = \Sigma_m(\omega) \delta_{x,1} \delta_{x',1} \delta_{s,1} \delta_{s',1}, \quad (\text{C4})$$

$$[\tilde{\Sigma}_m^R]_{x,s;x',s'} = \Sigma_m(\omega) \delta_{x,N_x} \delta_{x',N_x} \delta_{s,2} \delta_{s',2}. \quad (\text{C5})$$

$\Sigma_m(\omega)$ is defined as follows,

$$\Sigma_m(\omega) = \begin{cases} \frac{\eta_c^2}{\eta_x} \left[\frac{\bar{\omega}_m}{2\eta_x} + \sqrt{\frac{\bar{\omega}_m^2}{4\eta_x^2} - 1} \right], & \text{if } \bar{\omega}_m < -2\eta_x, \\ \frac{\eta_c^2}{\eta_x} \left[\frac{\bar{\omega}_m}{2\eta_x} - i \sqrt{1 - \frac{\bar{\omega}_m^2}{4\eta_x^2}} \right], & \text{if } |\bar{\omega}_m| < 2\eta_x, \\ \frac{\eta_c^2}{\eta_x} \left[\frac{\bar{\omega}_m}{2\eta_x} - \sqrt{\frac{\bar{\omega}_m^2}{4\eta_x^2} - 1} \right], & \text{if } \bar{\omega}_m > 2\eta_x, \end{cases} \quad (\text{C6})$$

with $\bar{\omega}_m = \omega - 2\eta_y \cos k_m$.

The steady-state two-point correlation matrix of the system can be expressed as [39]

$$C_{x,y,s;x',y',s'} = \langle c_s^\dagger(x, y) c_{s'}(x', y') \rangle, \quad (\text{C7})$$

where $\langle \cdot \rangle$ denotes the expectation value in the non-equilibrium steady state. Using Eq. (B7), the correlation matrix can be written as,

$$\begin{aligned} C_{x,y,s;x',y',s'} &= \frac{1}{N_y} \sum_{m,m'=1}^{N_y} e^{i(k_m y - k_{m'} y')} \langle \tilde{c}_{s,m}^\dagger(x) \tilde{c}_{s',m'}(x') \rangle, \\ &= \frac{1}{N_y} \sum_{m=1}^{N_y} e^{ik_m(y-y')} \tilde{C}_{x,s;x',s'}^m, \end{aligned} \quad (\text{C8})$$

where we have used the fact that the Fourier modes along the y -direction are uncorrelated and hence $\langle \tilde{c}_{a,m}^\dagger(x) \tilde{c}_{b,m'}(x') \rangle = \tilde{C}_{x,a;x',b}^m \delta_{m,m'}$. We note that \tilde{C}^m is the correlation matrix for the effective 1D chains and can be expressed as [39],

$$\tilde{C}^m = \int_{-\infty}^{\infty} d\omega [\mathcal{A}^{m,L}(\omega) f^L(\omega) + \mathcal{A}^{m,R}(\omega) f^R(\omega)], \quad (\text{C9})$$

where

$$\mathcal{A}^{m,L/R}(\omega) = 2\pi \tilde{\mathcal{G}}^m(\omega) \tilde{\Gamma}_m^{L/R}(\omega) (\tilde{\mathcal{G}}^m(\omega))^\dagger, \quad (\text{C10})$$

$\tilde{\Gamma}_m^{L/R}(\omega) = (\tilde{\Sigma}_m^{L/R}(\omega) - [\tilde{\Sigma}_m^{L/R}(\omega)]^\dagger)/(2\pi i)$ and $f^{L/R}(\omega) = f(\omega, \mu_{L/R}, T_{L/R})$ are the Fermi distribution functions of the two reservoirs.

The expression for the steady-state current along the bond connecting the sites $\mathbf{x} = (x, y)$ and $\mathbf{x}' = (x', y')$ follows from the continuity equation and can be written as,

$$J_{\mathbf{x}, \mathbf{x}'} = -2 \sum_{s, s'=1}^2 \text{Im} \{ H^S[\mathbf{x}, s; \mathbf{x}', s'] C_{\mathbf{x}, s; \mathbf{x}', s'} \}. \quad (\text{C11})$$

We note here that while Eq. (C11) can be used to compute the current in the CI, the same equation with a slight modification can also be used to compute the current inside the metallic region [37]. The main point to note is that in the nonequilibrium steady state of the Lead-CI-Lead setup, the state of the leads has also evolved and therefore contains the full information about the scattering states of the full system. Therefore, we consider a Lead-Metal-CI-Metal-Lead setup where the Hamiltonian of the metals is now identical to that of leads, and the contacts of the metal with the CI are identical to the contacts of the lead with CI in the Lead-CI-Lead system. In other words, we include a part of the leads and their contacts into the wire Hamiltonian, H^S , and then use the NEGF formalism. The current densities in the two setups are identical because of the uniqueness of the NESS. We have used this idea in Fig. (3) of the main text to compute the current density inside the leads and shown that it is identical to what we obtain from the scattering states of the Lead-CI-Lead system.

The edge modes are localized either at the left or at the right boundary of the cylinder. Hence, they do not carry any current along the x -direction, so we focus exclusively on the total current in the y -direction, which is given by

$$\begin{aligned} J_y &= \sum_{x=1}^{N_x} J_{x, y; x, y+1}, \\ &= -2 \sum_{x=1}^{N_x} \sum_{s, s'=1}^2 \text{Im} \{ H_{x, y, s; x, y+1, s'}^S C_{x, y, s; x, y+1, s'} \}. \end{aligned} \quad (\text{C12})$$

The subscript on J_y only labels the direction of the current, and it does not depend on y because of the cylindrical symmetry of the system.

Substituting Eq. (C9) in Eq. (C8) and using the result in Eq. (C13), J_y can be rewritten as [37],

$$J_y = \sum_{x=1}^{N_x} \sum_{m=1}^{N_y} \int_{-\infty}^{\infty} d\omega [F_{x,x}^{m,L}(\omega) f^L(\omega) + F_{x,x}^{m,R}(\omega) f^R(\omega)], \quad (\text{C14})$$

where,

$$F_{x,x}^{m,L/R}(\omega) = -\frac{1}{N_y} \sum_{s, s'=1}^2 \text{Im} \left[e^{-ik_m} (\sigma_x + i\sigma_z)_{s, s'} \mathcal{A}_{x, s; x, s'}^{m, L/R} \right]. \quad (\text{C15})$$

As mentioned in the main text, we work at zero temperature and in the linear response regime i.e. $\mu_R = \mu$

and $\mu_L = \mu + \Delta\mu$. Then, the steady-state current expression in Eq. (C14) naturally decomposes into two parts, an equilibrium part J_{eq} and an excess part ΔJ_y [37],

$$J_y = J_{eq} + \Delta J_y, \quad (\text{C16})$$

where

$$J_{eq} = \sum_{x=1}^{N_x} \sum_{m=1}^{N_y} \int_{-\infty}^{\mu} d\omega [F_{x,x}^{m,L}(\omega) + F_{x,x}^{m,R}(\omega)], \quad (\text{C17})$$

and

$$\Delta J_y = \sum_{x=1}^{N_x} \sum_{m=1}^{N_y} F_{x,x}^{m,L}(\mu) \Delta\mu. \quad (\text{C18})$$

In Eq. (C17), the integration from $-\infty$ to μ includes contributions from both bulk and edge states. The bulk states appear in left and right moving pairs whose currents cancel each other. Within the band gap, the two chiral edge modes at each μ (see Fig. 4 in the main text) are exponentially localized at the cylinder's opposite boundaries and propagate with opposite chirality. Thus, their contributions to the equilibrium current also cancel each other, giving $J_{eq} = 0$. Hence, only the nonequilibrium excess current ΔJ_y driven by $\Delta\mu$ remains, which is given by Eq. (C18). This current can be used to define Hall conductance as,

$$G_H(\mu) = \lim_{\Delta\mu \rightarrow 0} \frac{\Delta J_y}{\Delta\mu}. \quad (\text{C19})$$

We use Eq. (C15) and Eq. (C18) in Eq. (C19) and evaluate the imaginary part to express the Hall conductance as,

$$G_H(\mu) = \frac{1}{N_y} \sum_{x=1}^{N_x} \sum_{m=1}^{N_y} \sum_{s, s'=1}^2 R_{s, s'}(k_m) \mathcal{A}_{x, s; x, s'}^{m, L}(\mu), \quad (\text{C20})$$

where

$$R_{s, s'}(k_m) = (\sigma_z \cos k_m - \sigma_x \sin k_m)_{s, s'}. \quad (\text{C21})$$

Using Eq. (C4), (C6) and (C10), Eq. (C20) further simplifies to,

$$G_H(\mu) = \frac{2}{N_y} \sum_{x=1}^{N_x} \sum_{m=1}^{N_y} \sum_{s, s'=1}^2 \gamma_m [\tilde{\mathcal{G}}^m]_{x, s; 1, 1}^\dagger R_{s, s'}(k_m) \tilde{\mathcal{G}}_{x, s'; 1, 1}^m, \quad (\text{C22})$$

where $\gamma_m = \text{Im}[\Sigma_m(\mu)]$. Note that, in the above equation, we have suppressed μ dependence from γ_m and elements of $\tilde{\mathcal{G}}^m$. Eq. (C22) can be written as,

$$G_H(\mu) = \frac{2}{N_y} \sum_{x=1}^{N_x} \sum_{m=1}^{N_y} \gamma_m \mathbf{g}_{x1}^\dagger(k_m) R(k_m) \mathbf{g}_{x1}(k_m), \quad (\text{C23})$$

where we have defined

$$\mathbf{g}_{x1}(k_m) = \left(\tilde{\mathcal{G}}_{x, 1; 1, 1}^m \quad \tilde{\mathcal{G}}_{x, 2; 1, 1}^m \right)^T = \left(g_{x1}^{(1)} \quad g_{x1}^{(2)} \right)^T. \quad (\text{C24})$$

We now evaluate Eq. (C23) in the thermodynamic limit, i.e. $N_x, N_y \rightarrow \infty$. In this limit, the Hall conductance is given by Eq. (6) of the main text. We derive this expression using the transfer matrix approach in the next section.

Appendix D: Transfer matrix formulation and G_H in the thermodynamic limit

The transfer matrix approach recursively relates the matrix elements of the Green's function that appear in Eq. (C23). For the effective 1D system the Green's function $\tilde{G}^m(\mu)$ satisfies the following identity,

$$(\mu - \tilde{H}_m^S - \tilde{\Sigma}_m^L(\mu) - \tilde{\Sigma}_m^R(\mu))\tilde{G}^m(\mu) = \mathbb{I}. \quad (D1)$$

Note that the column vectors \mathbf{g}_{x1} required in Eq. (C23) are the elements of the first column of $\tilde{G}^m(\mu)$ which we denote by the vector $(g_{11}^{(1)}, g_{11}^{(2)}, g_{21}^{(1)}, \dots, g_{N_x 1}^{(1)}, g_{N_x 1}^{(2)})^T$. By equating the first columns on both sides of Eq. (D1), we obtain the following set of equations,

$$(\mu - a - \Sigma_m(\mu))g_{11}^{(1)} - bg_{11}^{(2)} = 1, \quad (D2)$$

$$-bg_{x-1,1}^{(1)} + (\mu + a)g_{x-1,1}^{(2)} - g_{x,1}^{(1)} = 0, \quad (2 \leq x \leq N), \quad (D3)$$

$$-g_{x-1,1}^{(1)} + (\mu - a)g_{x,1}^{(1)} - bg_{x,1}^{(2)} = 0, \quad (2 \leq x \leq N), \quad (D4)$$

$$-bg_{N_x 1}^{(1)} + (\mu + a - \Sigma_m(\mu))g_{N_x 1}^{(2)} = 0. \quad (D5)$$

where we have dropped k_m dependence from $a(k_m)$ and $b(k_m)$, for brevity.

Eq. (D2) and Eq. (D5) can be written in the matrix form as,

$$\begin{pmatrix} 1 \\ g_{11}^{(1)} \end{pmatrix} = \Omega_L \mathbf{g}_{11} \quad (D6)$$

and

$$\mathbf{g}_{N_x 1} = \Omega_R \begin{pmatrix} g_{N_x 1}^{(2)} \\ 0 \end{pmatrix}, \quad (D7)$$

respectively. Ω_L and Ω_R are defined as,

$$\Omega_L = \begin{pmatrix} \mu - a - \Sigma_m(\mu) & -b \\ 1 & 0 \end{pmatrix}, \quad (D8)$$

$$\Omega_R = \begin{pmatrix} \frac{\mu + a - \Sigma_m(\mu)}{b} & -1 \\ 1 & 0 \end{pmatrix}. \quad (D9)$$

Similarly, using Eq. (D3) and Eq. (D4), we obtain,

$$\mathbf{g}_{x-1,1} = \Omega \mathbf{g}_{x,1}, \quad (2 \leq x \leq N_x) \quad (D10)$$

where

$$\Omega = \begin{pmatrix} \frac{\mu^2 - a^2 - 1}{b} & -(\mu + a) \\ \mu - a & -b \end{pmatrix}. \quad (D11)$$

We note that Ω_L and Ω_R are the boundary transfer matrices, encoding the details of the reservoirs and their couplings to the CI, while Ω denotes the bulk transfer matrix of the CI, which depends on μ and k_m . Eq. (D10) can be recursively used to write \mathbf{g}_{x1} in terms of $\mathbf{g}_{N_x 1}$ as,

$$\mathbf{g}_{x1} = \Omega^{N-x} \mathbf{g}_{N_x 1}. \quad (D12)$$

Moreover, the two components of $\mathbf{g}_{N_x 1}$ are related by Eq. (D5) which gives,

$$\mathbf{g}_{N_x 1} = g_{N_x 1}^{(2)} |\xi_m(\mu)\rangle. \quad (D13)$$

where,

$$|\xi_m(\mu)\rangle = \boldsymbol{\xi}_m(\mu) = \begin{pmatrix} \frac{\mu + a - \Sigma_m(\mu)}{b} \\ 1 \end{pmatrix}. \quad (D14)$$

Here, for notational convenience in subsequent calculations, we have introduced bra-ket notation for row and column vectors, respectively. Substituting Eq. (D12) and (D13) in Eq. (C23), the Hall conductance can be written compactly as

$$G_H(\mu) = \frac{2}{N_y} \sum_{m=1}^{N_y} \gamma_m \langle \xi_m(\mu) | M(\mu, k_m) | \xi_m(\mu) \rangle, \quad (D15)$$

where

$$M(\mu, k_m) = |g_{N_x 1}^{(2)}|^2 \sum_{x=1}^{N_x} (\Omega^T)^{N_x-x} R \Omega^{N_x-x}. \quad (D16)$$

Eq. (D15) rewrites the Hall conductance entirely in terms of the products of 2×2 transfer matrices Ω_L , Ω and Ω_R . The dependence on N_x now appears only as the exponents on these small matrices, and the dependence on N_y appears in the sum over m in Eq. (D15). The only quantity left to determine now is $g_{N_x 1}^{(2)}$. Using Eq. (D6)-(D11), we can write

$$\begin{pmatrix} 1 \\ g_{11}^{(1)} \end{pmatrix} = \Omega_L \Omega^{N_x-1} \Omega_R \begin{pmatrix} g_{N_x 1}^{(2)} \\ 0 \end{pmatrix}. \quad (D17)$$

Using the upper row of Eq. (D17), we get

$$g_{N_x 1}^{(2)} = (\Omega_L \Omega^{N_x-1} \Omega_R)_{11}^{-1}. \quad (D18)$$

Let us denote the eigenvalues of Ω by λ_1, λ_2 and let the corresponding right and left eigenvectors be $|\lambda_i^R\rangle$ and $\langle \lambda_i^L|$ with $i = 1, 2$. These are normalized as per the usual bi-orthogonality condition $\langle \lambda_i^L | \lambda_j^R \rangle = \delta_{ij}$. Explicitly the eigenvalues are:

$$\lambda = \lambda_{1,2} = \frac{\Delta \pm \sqrt{\Delta^2 - 4}}{2}, \quad (D19)$$

where $\Delta = \frac{\mu^2 - a^2 - b^2 - 1}{b}$ and we use the convention such that $|\lambda_1| < |\lambda_2|$. We can now simplify Eq. (D18) using the spectral decomposition of Ω :

$$\Omega = \lambda_1 P_1 + \lambda_2 P_2, \quad (D20)$$

where P_1 and P_2 are projectors defined as,

$$P_i = |\lambda_i^R\rangle\langle\lambda_i^L|, \quad i = 1, 2. \quad (\text{D21})$$

Using Eq. (D20) in Eq. (D18), $g_{N_x 1}^{(2)}$ can be written as,

$$g_{N_x 1}^{(2)} = \frac{1}{\lambda_1^{N_x-1}\alpha + \lambda_2^{N_x-1}\beta}, \quad (\text{D22})$$

where $\alpha = (\Omega_L P_1 \Omega_R)_{11}$ and $\beta = (\Omega_L P_2 \Omega_R)_{11}$. The spectral decomposition can further be used to simplify Eq. (D16) to get,

$$M(\mu, k_m) = \sum_{x=1}^{N_x} [d_1(x) P_1^T R P_1 + d_2(x) P_2^T R P_2 + d_3(x) (P_1^T R P_2 + P_2^T R P_1)]. \quad (\text{D23})$$

The coefficients $d_1(x), d_2(x), d_3(x)$ are given by

$$d_1(x) = |g_{N_x 1}^{(2)}|^2 \lambda_1^{2(N_x-x)}, \quad (\text{D24})$$

$$d_2(x) = |g_{N_x 1}^{(2)}|^2 \lambda_2^{2(N_x-x)}, \quad (\text{D25})$$

$$d_3(x) = |g_{N_x 1}^{(2)}|^2 N_x. \quad (\text{D26})$$

For the Fermi level in the band gap, eigenvalues λ_1 and λ_2 are real and labeled such that $|\lambda_1| < 1 < |\lambda_2|$. From Eq. (D22), it then follows that $|g_{N_x 1}^{(2)}|^2 \sim |\beta|^{-2} \lambda_2^{-2(N_x-1)}$ for large N_x . Consequently, the coefficients $d_1(x)$ and $d_3(x)$ vanish in the limit $N_x \rightarrow \infty$, while $d_2(x)$ converges to $|\beta|^{-2} \lambda_2^{-2x}$. As a result, in this limit the expression for $M(\mu, k_m)$ in Eq. (D24) simplifies to

$$\lim_{N_x \rightarrow \infty} M(\mu, k_m) = \frac{1}{|\beta|^2} \left(\lim_{N_x \rightarrow \infty} \sum_{x=1}^{N_x} \lambda_2^{-2(x-1)} \right) P_2^T R P_2, \quad (\text{D27})$$

$$= \frac{1}{|\beta|^2} \frac{1}{1 - \lambda_1^2} P_2^T R P_2. \quad (\text{D28})$$

Substituting Eq. (D28) into the expression for Hall conductance Eq. (D15) and then taking the limit $N_y \rightarrow \infty$ by appropriately replacing the sum over m with an integral over k , we get

$$G_H(\mu) = \frac{1}{\pi} \int_0^{2\pi} dk \frac{\gamma(\mu, k)}{|\beta(k)|^2} \frac{\langle \xi_k | P_2^T R P_2 | \xi_k \rangle}{1 - \lambda_1^2(k)}. \quad (\text{D29})$$

To simplify it further, we notice that,

$$\beta = (\Omega_L P_2 \Omega_R)_{11}, \quad (\text{D30})$$

$$= \begin{pmatrix} 1 & 0 \end{pmatrix} \Omega_L |\lambda_2^R\rangle\langle\lambda_2^L| \Omega_R \begin{pmatrix} 1 \\ 0 \end{pmatrix}, \quad (\text{D31})$$

$$= -b\langle \xi_k(-\mu) | \lambda_2^R(\mu) \rangle \langle \lambda_2^L(\mu) | \xi_k(\mu) \rangle. \quad (\text{D32})$$

So, $|\beta|^2 = b^2 |\langle \xi_k(-\mu) | \lambda_2^R(\mu) \rangle|^2 |\langle \xi_k(\mu) | \lambda_2^L(\mu) \rangle|^2$ which can be used in Eq. (D29) with the fact that $P_2 = |\lambda_2^R\rangle\langle\lambda_2^L|$ to give

$$G_H(\mu) = \frac{1}{\pi} \int_0^{2\pi} dk \frac{\gamma(\mu, k)}{\tilde{\beta}(k)} \frac{1}{1 - \lambda_1^2(k)} \langle \lambda_2^R | R | \lambda_2^R \rangle, \quad (\text{D33})$$

where $\tilde{\beta}(k) = b^2 |\langle \xi_k(-\mu) | \lambda_2^R(\mu) \rangle|^2$. Furthermore, we express $\tilde{\beta}(k)$ and $\langle \lambda_2^R | R | \lambda_2^R \rangle$ in terms of the components of the eigenvector $|\lambda_2^R\rangle = \begin{pmatrix} v_1 & v_2 \end{pmatrix}^T$ and obtain the following

$$\langle \lambda_2^R | R | \lambda_2^R \rangle = (\mu_w - b(k))(v_1^2 - v_2^2) + 2a(k)v_1 v_2, \quad (\text{D34})$$

$$\tilde{\beta}(k) = \gamma^2(\mu, k)v_1^2 + [(a(k) - \mu + \Lambda(k))v_1 + b(k)v_2]^2, \quad (\text{D35})$$

where $\Lambda(\mu, k) = \text{Re}[\Sigma_k(\mu)]$. By substituting Eq. (D34), and Eq. (D35) in Eq. (D33) we obtain Eq. (5) of the main text,

$$G_H(\mu) = \frac{1}{\pi} \int_0^{2\pi} \frac{\gamma(\mu, k)}{\gamma^2(\mu, k) + g^2(\mu, k)} h(\mu, k) dk, \quad (\text{D36})$$

where $g(\mu, k)$ and $h(\mu, k)$ are given by,

$$g(\mu, k) = (a(k) - \mu) + \Lambda(\mu, k) + b(k)f(k), \quad (\text{D37})$$

$$h(\mu, k) = \frac{(b(k) - \mu_w)(1 - f^2(k)) - 2a(k)f(k)}{1 - \lambda_1^2(k)}, \quad (\text{D38})$$

with

$$f(k) = \frac{v_2}{v_1} = \frac{(\mu - a(k))}{\lambda_2(k) + b(k)}. \quad (\text{D39})$$

Appendix E: Special case of 1D leads ($\eta_y = 0$)

As discussed in the main text, for 1D leads, i.e. $\eta_y = 0$, the self energy becomes independent of k and $\frac{dg(k)}{dk} = h(k)$. This allows us to write the $G_H(\mu)$ as winding of a phase $\phi(k)$ as

$$G_H = \frac{1}{2\pi} \int_0^{2\pi} \partial_k \phi(k) dk \quad (\text{E1})$$

where $\phi(k) = 2 \tan^{-1} \frac{g(k)}{\gamma}$.

Proof of non-zero winding of $\phi(\mu, k)$ in the topological regime: We rewrite the integral in Eq. (E1) in terms of $z = e^{i\phi(\mu, k)}$ as,

$$G_H(\mu) = \frac{1}{2\pi i} \int_C \frac{dz}{z}. \quad (\text{E2})$$

where the C is the closed contour traced by z as k varies from 0 to 2π . Thus, $G_H(\mu) = \pm 1$ or vanishes depending on whether or not $\phi(\mu, k)$ winds around the origin in the counterclockwise or clockwise direction, respectively, as k varies from 0 to 2π .

$\phi(\mu, k)$ will wind around the origin iff its range covers the entire region $-\pi \leq \phi(\mu, k) \leq \pi$ for $0 \leq k < 2\pi$. The range of $\phi(\mu, k)$ is dictated by the range of $g(\mu, k)$. For $\phi(\mu, k) \in (-\pi, \pi)$, $g(\mu, k) \in (-\infty, \infty)$. We show that $g(\mu, k) \in (-\infty, \infty)$ only in the topological regime. To that end, we substitute f from Eq. (D39) in Eq. (D37) to write $g(\mu, k)$ as,

$$g(\mu, k) = c(\mu, k) + \Lambda, \quad (\text{E3})$$

where

$$c(\mu, k) = \frac{(a - \mu)\lambda_2}{b + \lambda_2}. \quad (\text{E4})$$

Note that Λ is independent of k , thus $g(\mu, k)$ is just a shift of the function $c(\mu, k)$. Therefore, the ranges of the two are the same. $c(\mu, k)$ is a smooth and continuous function of k , except for possible singularities where $b = -\lambda_2$. We now examine these points.

Eq. (D19) implies that $b = -\lambda_2 \Rightarrow a = \pm\mu$. Note an important point here: $b = -\lambda_2$ implies $a = \pm\mu$, but the converse is not true. Given $a = \pm\mu$ gives $\Delta = -(b + 1/b)$ and thus λ_2 is by definition either $-b$ or $-1/b$ depending on whether $|b| > 1$ or $|b| < 1$, respectively. Note that since μ lies inside the bulk gap, given by $\min\{2 - \mu_w, \mu_w\}$, $|\mu| < 1$. Therefore, $a = \pm\mu$ will always be satisfied for four different k values lying in the four quadrants. Let the four solutions be θ_p where $p = 1, 2, 3, 4$ denotes the quadrant in which the solution lies. At these four solutions, $|b|$ can be greater than or less than 1, thus we have the following cases,

- I: For $|b| > 1$ and $a = -\mu$, $c(\mu, k)$ blows up, as its denominator vanishes, but the numerator is finite. Furthermore, note that the $c(\mu, k) \sim \frac{1}{k - \theta_p}$, where $k = \theta_p$ where the denominator vanishes. Thus, $c(\mu, k) \rightarrow \pm\infty$ for the two directions of approaching $k = \theta_p$.
- II: For $|b| > 1$ and $a = \mu$, both the numerator and denominator of $c(\mu, k)$ vanish. Then, using L'Hopital's rule, it can be shown that $c(\mu, k)$ is finite.
- III: For $|b| < 1$ and $a = -\mu$, $c(\mu, k)$ as its numerator and denominator are finite.
- IV: For $|b| < 1$ and $a = \mu$, $c(\mu, k)$ vanishes as the numerator vanishes.

Out of the above cases, only case I and case IV are of interest. This is because if both cases occur as k varies from 0 to 2π , then the range of $c(k)$ and $g(\mu, k)$ is given by $(-\infty, \infty)$, thereby $\phi(k) \in (-\pi, \pi)$. This implies that $z = e^{i\phi(k)}$ winds around the origin as k goes from 0 to 2π . We now argue that this only happens in the topological regime.

Let us consider the topological regime with $\mu_w \in (0, 2)$. For $\mu > 0$ we have

- For $k = \theta_2$, $a = \mu$ and $b = \mu_w - \sqrt{1 - \mu^2}$. For $\mu < \min\{2 - \mu_w, \mu_w\}$, $|b| < 1$. Thus, the conditions for case IV are satisfied.
- For $k = \theta_4$, $a = -\mu$ and $b = \mu_w + \sqrt{1 - \mu^2}$. For $\mu < \min\{2 - \mu_w, \mu_w\}$, $|b| > 1$. Therefore, case I is satisfied.

Thus, in the topological regime $g(\mu, k)$ takes values from $-\infty$ to ∞ which gives the range of $\phi(k)$ to be $(-\pi, \pi)$.

This implies that the contour C in Eq. (E2) is just a unit circle that encloses the origin. Similar arguments can be repeated for $\mu_w \in (-2, 0)$.

Now let us consider the non-topological regime, $\mu_w > 2$. In this case, clearly $|b| > 1$ for all θ_p . Hence, $g(\mu, k)$ is finite for $a = \mu$ and blows up for $a = -\mu$. Since $g(\mu, k)$ never vanishes for the non-topological regime but does blow up, $\phi(k)$ lies in the interval (ϕ_-, ϕ_+) which contains $k = \pi$. This means C is a contour where z traces out an arc of a unit circle and then retraces it back, giving $G_H = 0$. Fig. A1 shows the contour for the topological and the non-topological parameter regimes.

Appendix F: Hall conductance via scattering approach

In this section, we obtain the wavefunction of the scattering states for a lead-CI system, and use it to calculate the local Hall conductance given in Eq. (10) of the main text. We also show that the phase of the reflection coefficient is related to $\phi(k)$, defined in Eq. (7), which gives the winding number identified with the Hall conductance.

1. Scattering state solution

We consider a semi-infinite SBHZ model connected to a semi-infinite 2D metallic lead with periodic boundary conditions (PBC) along the y -direction. The solution for the 1D metallic lead case can then be obtained simply by setting $\eta_y = 0$.

We assume that the wavefunction of the scattering state of energy ϵ to be of the form $\zeta_{q,k}(x, y) = \Psi_{q,k}(x)e^{iky}$, where we define $\Psi_{q,k}(x)$ as follows,

$$\Psi_{q,k}(x) = \begin{cases} \psi_M(x), & x \leq 0, \\ \begin{pmatrix} \psi_1(x) \\ \psi_2(x) \end{pmatrix} & x > 0. \end{cases} \quad (\text{F1})$$

$\psi_M(x)$ is the wavefunction inside the leads and $\begin{pmatrix} \psi_1(x) \\ \psi_2(x) \end{pmatrix}^T$ is the wavefunction inside the CI. We will see shortly that q labels the momentum in the x direction of the incoming electron incident on the junction.

Following the standard scattering approach, we first consider the eigenvalue equation

$$\sum_{x'=-\infty}^{\infty} H_k[x, x']\Psi_{q,k}(x') = \epsilon\Psi_{q,k}(x), \quad (\text{F2})$$

in the bulk of the lead ($x < 0$) and the CI ($x > 0$). H_k is the Hamiltonian of the lead-CI system in the Fourier space. For the region inside the leads ($x < 0$), Eq. (F2) gives

$$\eta_x\psi_M(x+1) + 2\eta_y\cos k\psi_M(x) + \eta_x\psi_M(x-1) = \epsilon\psi_M(x), \quad (\text{F3})$$

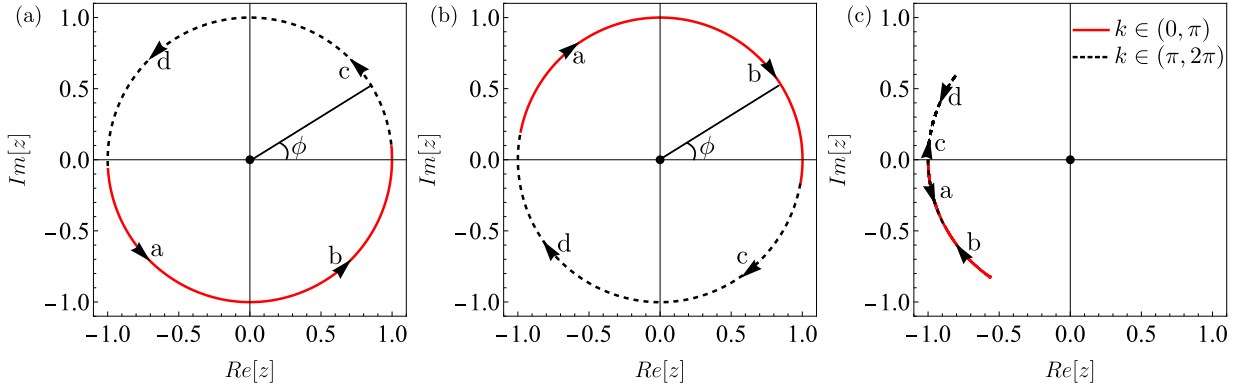


FIG. A1. Winding of the function $z(k) = e^{i\phi(k)}$ as k varies from 0 to 2π . (a) and (b) are for topological regimes with $\mu_w = 1$ and $\mu_w = -1$, respectively and (c) corresponds to the trivial regime with $\mu_w = 2.2$. The arrows labelled from a to d indicate the direction of change of $\phi(k)$ as k increases from 0 to 2π . The common parameters for the three panels are $\mu = 0.1$, $\eta_x = 1$ and $\eta_c = 1$.

and for the region inside the CI Eq. (F2) gives

$$\psi_2(x-1) + b\psi_2(x) + a\psi_1(x) = \epsilon\psi_1(x), \quad x \geq 2 \quad (\text{F4})$$

$$\psi_1(x+1) + b\psi_1(x) - a\psi_2(x) = \epsilon\psi_2(x), \quad x \geq 1 \quad (\text{F5})$$

We look for solutions of the following form:

$$\psi_M(x) = e^{iqx} + r e^{-iqx}, \quad x \leq 0, \quad (\text{F6})$$

$$\begin{pmatrix} \psi_1(x) \\ \psi_2(x) \end{pmatrix} = \begin{pmatrix} u \\ v \end{pmatrix} \lambda^{x-1}, \quad x > 0, \quad (\text{F7})$$

where u, v, r, λ are arbitrary coefficients to be determined. Physically, the above form represents a plane wave with momentum $q \in (0, \pi)$ incident at the junction, which is reflected with a reflection coefficient r and decays inside the CI. Substituting $\psi_M(x)$ from Eq. (F6) into Eq. (F3), (F4), (F5), we get

$$\epsilon = 2\eta_x \cos q + 2\eta_y \cos k, \quad (\text{F8})$$

while λ_1 (chosen as $|\lambda_1| < |\lambda_2|$) is given by

$$\lambda_{1,2} = \frac{\Delta \pm \sqrt{\Delta^2 - 4}}{2}, \quad (\text{F9})$$

where $\Delta = \frac{\epsilon^2 - a^2 - b^2 - 1}{b}$. Finally we also get

$$v/u = f(k) = \frac{\epsilon - a}{b + 1/\lambda_1} = \frac{\lambda_1 + b}{\epsilon + a}. \quad (\text{F10})$$

For the scattering state of the edge modes, ϵ lies inside the band gap of the CI, therefore $\lambda_{1,2}$ are real.

The remaining unknowns now are the coefficients u and r . These are fixed by the eigenvalue equation at the lead-CI junction given by,

$$\eta_x \psi_M(-1) + \eta_c \psi_1(1) = \epsilon \psi_M(0), \quad (\text{F11})$$

$$\eta_c \psi_M(0) + a\psi_1(1) + b\psi_2(1) = \epsilon \psi_1(1). \quad (\text{F12})$$

Putting the ansatz in Eq. (F6) and Eq. (F7) into Eq. (F11) and Eq. (F12) we obtain the following solution for u and r ,

$$r = \frac{-(c(k)e^{iq} + \frac{\eta_c^2}{\eta_x})}{c(k)e^{-iq} + \frac{\eta_c^2}{\eta_x}} = e^{i\chi(k)}, \quad (\text{F13})$$

$$u = \frac{2i\eta_c \sin q}{c(k)e^{-iq} + \frac{\eta_c^2}{\eta_x}}. \quad (\text{F14})$$

Note that e^{-iq} is related to the self energy as

$$\Sigma_m(\epsilon) = \frac{\eta_c^2}{\eta_x} e^{-iq}. \quad (\text{F15})$$

Using this relation in Eq. (F13), we get the phase of the reflection coefficient as,

$$\chi(k) = -2 \arctan \left(\frac{c\Lambda + \eta_c^4 \eta_x^{-2}}{c\gamma} \right). \quad (\text{F16})$$

Simple algebra using the definitions of $\phi(q, k)$ and $\chi(q, k)$ in the glossary of symbols shows that

$$\tan(\phi/2 + q) = \tan(\chi/2) \Rightarrow \partial_k \chi(k) = \partial_k \phi(k). \quad (\text{F17})$$

2. Hall Conductance

Having obtained the scattering states, we can compute the local current density along the y direction using the following expression,

$$j_y(x; q, k) = -2\text{Im}[\zeta_{q,k}^\dagger(x, y) H[x, y; x, y+1] \zeta_{q,k}(x, y+1)], \quad (\text{F18})$$

where $H[x, y; x, y+1]$ is the hopping strength in the y direction in the CI or lead Hamiltonian. Using the form of the wavefunction due to cylindrical symmetry, the current can be expressed as

$$j_y(x; q, k) = \Psi_{q,k}^\dagger(x) \hat{J}_y \Psi_{q,k}(x), \quad (\text{F19})$$

where

$$\hat{J}_y = \begin{cases} \sigma_z \cos k - \sigma_x \sin k & \text{for } x \geq 0, \\ -2\eta_y \sin k & \text{for } x < 0. \end{cases} \quad (\text{F20})$$

is the current operator corresponding to current along the y direction.

So, the total current due to scattering states filled upto the Fermi level μ is given by,

$$J_y(\mu, x) = \frac{1}{2\pi} \int_0^{2\pi} dk \int_0^{q_F} dq j_y(x; q, k) \Theta(\mu - \epsilon_{q,k}), \quad (\text{F21})$$

where $\epsilon_{q,k}$ is given by Eq. (F8). Differentiating Eq. (F21) with respect to μ , we can define *local* Hall conductance as,

$$\tilde{G}_H(\mu, x) = \frac{1}{2\pi} \int_0^{2\pi} dk \int_0^{q_F} dq j_y(x; q, k) \delta(\mu - \epsilon_{q,k}). \quad (\text{F22})$$

The Hall conductance is then given by

$$G_H(\mu) = G_H^{\text{lead}}(\mu) + G_H^{\text{CI}}(\mu), \quad (\text{F23})$$

where

$$G_H^{\text{lead}}(\mu) = \sum_{x=-\infty}^0 \tilde{G}_H(\mu, x), \quad (\text{F24})$$

is the contribution due to the leads and

$$G_H^{\text{CI}}(\mu) = \sum_{x=1}^{\infty} \tilde{G}_H(\mu, x). \quad (\text{F25})$$

is the contribution from the CI. The contribution from the lead and the CI can be evaluated by using the scattering state wavefunction given in Eq. (F6) and Eq. (F7) to get,

$$G_H^{\text{lead}}(\mu) = \sum_{x=-\infty}^0 \frac{-2\eta_y}{\pi} \int_0^{2\pi} dk \frac{\sin k \cos(2qx - \chi(k))}{\sqrt{4\eta_x^2 - (\mu - 2\eta_y \cos k)^2}} \quad (\text{F26})$$

$$G_H^{\text{CI}}(\mu) = \frac{1}{\pi} \int_0^{2\pi} dk \frac{\gamma(\mu, k)}{1 - \lambda_1^2} \frac{(1 - f^2) \cos k - 2af}{\gamma^2(\mu, k) + g^2(k)}. \quad (\text{F27})$$

Fig. 4 of the main text shows how contributions from lead and CI add up to 1 in the topological regime. Although the numerical computations clearly indicate that quantization is retained by including the contribution from the leads, an analytical proof of this fact is desirable. It is straightforward to see that the $G_H^{\text{CI}}(\mu)$ from Eq. (F27) is the same as $G_H(\mu)$ from Eq. (D36) using the NEGF approach, and for $\eta_y = 0$, $G_H^{\text{lead}}(\mu)$ vanishes. Therefore, the arguments from the main text give us the quantization of $G_H(\mu)$.